Opto-Electronic Science

Supplementary information

August 2024, Vol. 3, No. 8

DOI: 10.29026/oes.2024.240012

Multifunctional mixed analog/digital signal processor based on integrated photonics

Yichen Wu[1], Qipeng Yang[1], Bitao Shen[1], Yuansheng Tao[1], Xuguang Zhang[1], Zihan Tao[1], Luwen Xing[2], Zhangfeng Ge[3], Tiantian Li[4]*, Bowen Bai[1]*, Haowen Shu[1,5]* and Xingjun Wang[1,3,5,6]*

[1]State Key Laboratory of Advanced Optical Communication Systems and Networks, School of Electronics, Peking University, Beijing 100871, China; [2]College of Engineering, Peking University, Beijing 100871, China; [3]Peking University Yangtze Delta Institute of Optoelectronics, Nantong 226010, China; [4]School of Electronic Engineering, Xi'an University of Posts & Telecommunications, Xi'an 710121, China; [5]Frontiers Science Center for Nano-optoelectronics, Peking University, Beijing 100871, China; [6]Peng Cheng Laboratory, Shenzhen 518055, China.

*Correspondence: TT Li, E-mail: tiantianli@xupt.edu.cn; BW Bai, E-mail: bowenbai@pku.edu.cn; HW Shu, E-mail: haowenshu@pku.edu.cn; XJ Wang, E-mail: xjwang@pku.edu.cn

This file includes:

Supplementary information for this paper is available at https://doi.org/10.29026/oes.2024.240012

Section 1: The optical and RF response of the CMRR-DL system

The transmission characteristics of the CMRR-DL system can be described by the transmission matrixes of the components. The structure can by simplified to the model as shown in Fig. S1.

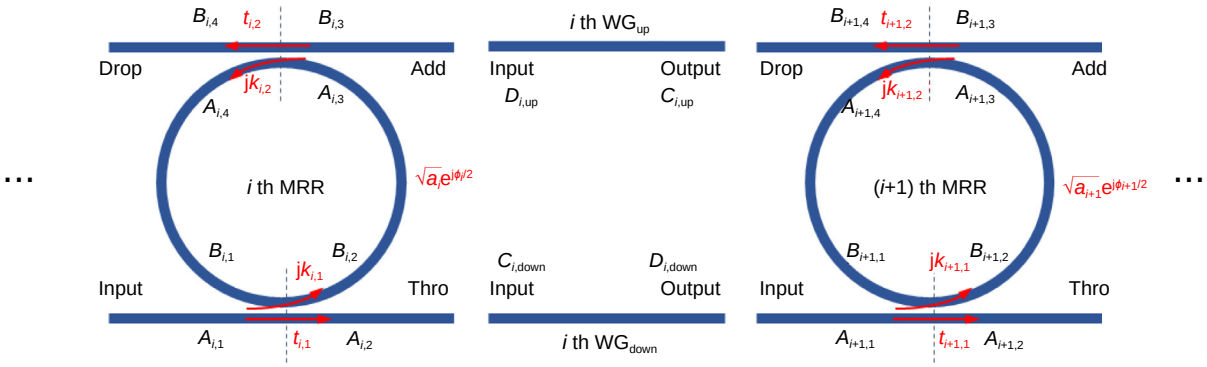

Fig. S1 | The simplified mode of the CMRR-DL system.

When the ring resonator is coupled to two waveguides, the transmission to the through and the drop port can be derived from CW operation and matching the fields[S1].

$$T_{\text{thro}} = \left|\frac{A_2}{A_1}\right|^2 = \frac{a^2t_2^2 - 2at_1t_2\cos\phi + t_1^2}{1 - 2at_1t_2\cos\phi + (at_1t_2)^2}\,, \tag{S1}$$

$$T_{\text{drop}} = \left|\frac{B_4}{A_1}\right|^2 = \frac{(1-t_1^2)(1-t_2^2)\,a}{1 - 2at_1t_2\cos\phi + (at_1t_2)^2}\,, \tag{S2}$$

In Eqs. (S1) and (S2), a represents the single-pass amplitude transmission, which is related to the power attenuation coefficient α[1/cm] as $a^2 = \exp(-\alpha L)$. $\phi = \beta L$ indicates the single-pass phase shift, with L the round trip length and β the propagation constant of circulating mode. The phase transmission functions can be expressed as

$$\Phi_{\text{thro}} = \arg\left(\frac{A_2}{A_1}\right) = \pi + \phi + \arctan\frac{t_1\sin\phi}{at_2 - t_1\cos\phi} + \arctan\frac{at_1t_2\sin\phi}{1 - at_1t_2\cos\phi}\,, \tag{S3}$$

$$\Phi_{\text{drop}} = \arg\left(\frac{B_4}{A_1}\right) = \pi + \phi/2 + \arctan\frac{at_1t_2\sin\phi}{1 - at_1t_2\cos\phi}\,. \tag{S4}$$

As for the delay line waveguide, the relationship between the output and input port can be expressed as:

$$T_{\text{wg}} = \left|\frac{D}{C}\right|^2 = \mathrm{e}^{-\alpha_{\text{wg}}L_{\text{wg}}}\,, \tag{S5}$$

$$\Phi_{\text{wg}} = \beta_{\text{wg}}L_{\text{wg}} \tag{S6}$$

Considering the CMRR-DL architecture, we have the two groups of equations to describe the fields of i th MRR-DL and its connection to the (i+1) th MRR-DL

$$\begin{cases} B_{i,4} = \sqrt{T_{\text{thro},i,\text{up}}}\,\mathrm{e}^{\mathrm{j}\Phi_{\text{thro},i,\text{up}}}B_{i,3} + \sqrt{T_{\text{drop},i,\text{up}}}\,\mathrm{e}^{\mathrm{j}\Phi_{\text{drop},i}}A_{i,1} \\ A_{i,2} = \sqrt{T_{\text{thro},i,\text{down}}}\,\mathrm{e}^{\mathrm{j}\Phi_{\text{thro},i,\text{down}}}A_{i,1} + \sqrt{T_{\text{drop},i,\text{down}}}\,\mathrm{e}^{\mathrm{j}\Phi_{\text{drop},i}}B_{i,3} \\ D_{i,\text{up}} = C_{i,\text{up}}\sqrt{T_{\text{wg},i,\text{up}}}\,\mathrm{e}^{\mathrm{j}\Phi_{\text{wg},i,\text{up}}} \\ D_{i,\text{down}} = C_{i,\text{down}}\sqrt{T_{\text{wg},i,\text{down}}}\,\mathrm{e}^{\mathrm{j}\Phi_{\text{wg},i,\text{down}}} \end{cases}, \tag{S7}$$

$$\begin{cases} B_{i,3} = D_{i,\text{up}} \\ A_{i,2} = C_{i,\text{down}} \\ A_{i+1,1} = D_{i,\text{down}} \\ C_{i,\text{up}} = B_{i+1,4} \end{cases}, \tag{S8}$$

By solving the equations of the system, we can derive the response of the system's drop port to the input which can be expressed as $E_{\text{output}}(\Omega) = \sqrt{T}\exp(\mathrm{j}\Omega t + \mathrm{j}\Phi)$. Here, Ω refers to the optical angular frequency, T and Φ are the power and phase response of the system. Due to the complexity arising from the large number of equations and variables, it is impractical to formulate a concise expression to describe the frequency equalization function of the system respectively. Therefore, we employ commercial software to model of the system's transmission property (Fig. S2(a)) and compute the RF response according to the optical response, taking into account the sidebands of MZI intensity modulation. The modulation sidebands and the carriers are coherently filtered by the system and detected by a high-bandwidth PD. The RF response can be expressed as[S2]

$$i(\omega_{\text{RF}}) \propto R\left\langle \left| \begin{array}{l} \dfrac{-\mathrm{j}}{2}J_1(m)\mathrm{e}^{\mathrm{j}(\Omega-\omega_{\text{RF}})t}\sqrt{T(\Omega-\omega_{\text{RF}})}\mathrm{e}^{\mathrm{j}\Phi(\Omega-\omega_{\text{RF}})} + J_0(m)\mathrm{e}^{\mathrm{j}(\Omega-\omega_{\text{RF}})t}\sqrt{T(\Omega)}\mathrm{e}^{\mathrm{j}\Phi(\Omega)} \\ +\dfrac{\mathrm{j}}{2}J_1(m)\mathrm{e}^{\mathrm{j}(\Omega_n+\omega_{\text{RF}})t}\sqrt{T(\Omega+\omega_{\text{RF}})}\mathrm{e}^{\mathrm{j}\Phi(\Omega+\omega_{\text{RF}})} \end{array} \right|^2 \right\rangle . \tag{S9}$$

To demonstrate the capability of generating diverse RF responses, we set the positions of resonances peaks to distribute randomly and uniformly by adjusting the single-pass phase shift in MRRs as shown in Table S1. Figure S2(b, c) illustrates various optical transmissions and RF responses resulting from different distribution.

Table S1 | The random single-round phase in MRRs (rad).

MRR ID Random ID	1	2	3	4	5	6	7	8	9
1	568.74	566.43	570.30	564.70	567.17	566.82	569.17	569.35	565.63
2	567.48	567.21	568.44	568.83	569.10	566.18	568.64	568.49	565.49
3	565.22	567.54	570.36	566.57	568.07	565.86	569.08	566.05	567.58
4	568.76	569.93	570.35	567.84	565.34	565.40	566.07	569.63	566.05
5	569.47	565.98	570.17	566.63	565.69	566.03	568.26	567.38	566.64
6	569.57	568.07	567.85	570.10	566.24	569.12	569.10	566.82	567.96
7	564.96	564.82	567.74	569.25	570.20	565.29	567.97	567.36	564.57
8	566.55	565.48	569.34	566.39	567.72	565.50	568.17	566.10	568.49
9	568.70	569.06	567.24	565.00	565.89	570.07	565.42	569.54	567.78
10	570.58	564.97	567.20	565.14	570.37	564.52	569.23	569.49	569.80
11	565.01	566.93	566.08	569.38	567.13	570.06	565.60	566.10	565.38
12	565.32	569.80	568.03	567.85	565.38	569.70	568.29	566.64	567.63
13	566.95	564.96	565.96	565.25	565.62	565.96	567.04	564.80	570.01
14	570.26	567.49	567.48	566.56	569.99	566.75	565.17	569.26	566.87
15	565.97	566.96	565.08	565.30	570.25	570.33	568.01	564.86	565.93
16	566.65	569.51	564.59	564.76	565.52	568.46	568.96	568.45	567.25
17	567.83	566.30	569.04	565.65	568.69	565.61	566.74	568.31	569.26
18	564.99	570.17	569.23	567.47	567.16	567.22	566.36	567.60	567.61
19	569.49	569.35	568.43	566.81	569.45	567.75	566.63	570.23	569.84
20	567.85	568.30	568.08	565.76	566.33	567.37	565.90	569.65	565.68
21	565.87	565.54	565.88	567.15	566.39	570.13	567.12	565.62	570.02
22	570.48	567.17	565.17	566.07	566.99	568.13	566.09	568.18	568.84
23	565.85	565.21	566.30	566.44	567.08	567.59	565.01	566.10	569.39
24	564.67	570.17	568.95	567.48	568.03	565.94	567.30	570.38	567.83
25	567.68	565.91	567.48	568.30	568.64	566.91	566.74	570.53	564.72

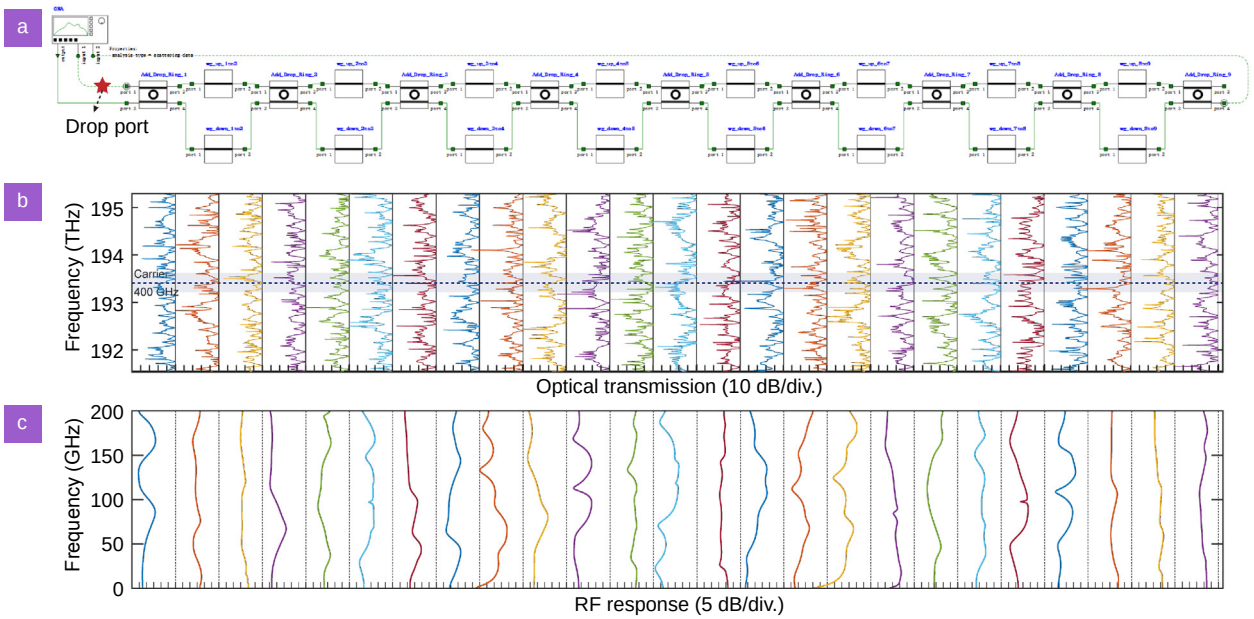

Fig. S2 | Simulated results of the CMRR-DL system in the frequency-domain. (**a**) The model built in software. (**b**) Optical transmission and (**c**) RF responses with random single-pass phase shift of 9 MRRs.

Section 2: Characteristics of the weight precision

Weight precision typically denotes the number of discrete levels attainable. In our system, the number of discrete levels can be expressed as[S3]

$$N = \frac{\omega_{\max} - \omega_{\min}}{2|\omega - \hat{\omega}|_{\max}}, \tag{S10}$$

where ω and $\hat{\omega}$ are the measured and target weight, $|\omega - \hat{\omega}|_{\max}$ indicates the maximum value of the errors. Given that the error can be positive or negative, the minimum weight interval that can be distinguished is $2|\omega - \hat{\omega}|_{\max}$. In our system, $\omega_{\max} = 1$, $\omega_{\min} = 0$, then the effective bit resolution can be written as

$$\log_2(N) = \log_2\left(\frac{1}{2|\omega - \hat{\omega}|_{\max}}\right). \tag{S11}$$

Then, we measured the transmission errors of each MRR channel individually. While one channel is being tuned to its target values using the Gradient-Descent algorithm, the other channels are set with a transmission list of all combination of (0, 0.33, 0.66, 1) to simulate the inner cross talk, ensuring the credibility of our measurements. Figure S4 shows

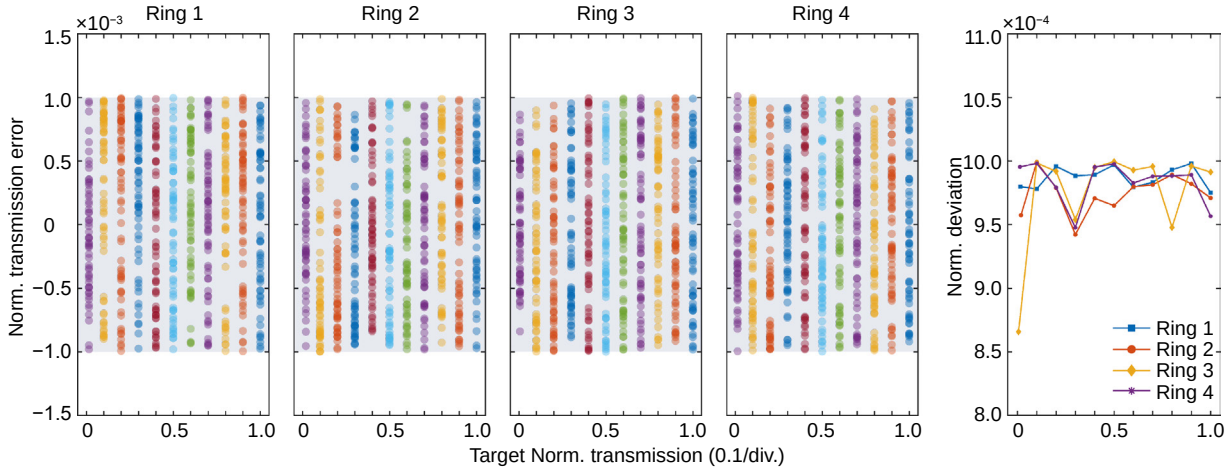

Fig. S3 | Detailed data of the measured transmission errors.

the aggregation of the errors derived from all the tested points, where almost all the points exhibit $|\omega - \hat{\omega}|_{\max} \approx 0.001$, showing the transmission control accuracy around 9-bit. The algorithm to calculate the accuracy is based on the Eq. (S11).

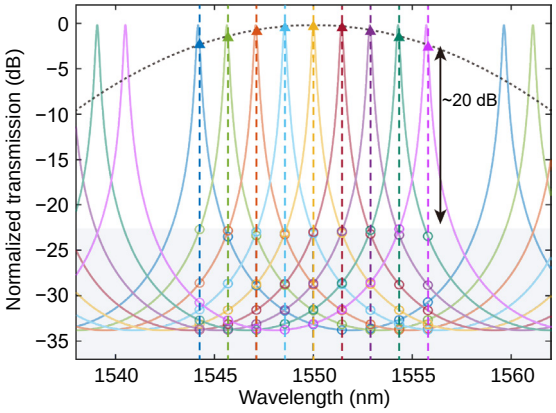

Fig. S4 | Optical transmission spectra of the used MRRs.

Section 3: The influence of channel crosstalk on the response of MPF

Considering a FIR MPF with N taps, the ideal frequency domain transfer function can be expressed as:

$$H(\omega) = \frac{s_o(j\omega)}{s_i(j\omega)} = \sum_{n=0}^{N-1} A_0(\lambda_n) T(\lambda_n) \, e^{-jn\omega\tau} = \sum_{n=0}^{N-1} a_n e^{-jn\omega\tau} , \tag{S12}$$

where ω is the RF angular frequency of the input microwave signal, a_n is the weight coefficient of each tap, . $A_0(\lambda_n)T(\lambda_n)$. is the optical power of the nth wavelength which can be measured by the optical spectrum analyzer (OSA) during the experiment, N is the total number of comb lines, τ is the time delay unit between the adjacent comb lines. Considering the parameter set that N is 9 and τ is equal to the delay value of the on-chip spiral delay line which is approximately 59 ps and the wavelength space $\Delta\lambda \approx 1.44$ nm ($\Delta\nu \approx 180$ GHz), the ideal frequency domain transfer is depicted in Fig. S6. Here to improve the main-to-sidelobe suppression ratio, the Gauss shape with $\sigma = 4$ is applied that the power of comb lines after the CMRR-DL system aliens to the expression:

$$P_n \propto \exp\left[\frac{(n - N/2)^2}{2\sigma^2}\right] , \tag{S13}$$

However, considering the realization of MRRs and delay lines. The function can be expressed more physically as:

$$H(\omega) = \sum_{n=0}^{N-1} \sum_{m=0}^{N-1} A_0(\lambda_m) T_n(\lambda_m) \, e^{-jn\omega\tau} , \tag{S14}$$

where m represents the mth wavelength and n represents the nth optical path determined by the MRR and the number of delay lines. As for a certain delay time, the optical power of all the N wavelength is considered due to the incomplete filtering effect of the MRRs. The optical transmission spectra of N MRRs are shown in Fig. S4, where the channels used for MWP are specified by the dashed lines with various colors. In Fig. S4, the circles mark the unexpected optical leakages and the extinct ratio is over 20 dB, the black dashed line illustrates the Gauss shape that the transmission of the used wavelengths fit. Utilizing the Eq. (S14) the frequency domain transfer is depicted in Fig. S6.

More accurately, there are unexpected resonators that are composed by two half parts of different MRRs and delay lines between them. When considering this factor, it is hard to express the complete function. We use commercial software to simulate the transmission properties by numerically calculating the transmission matrix. The amplitude and phase of the system at various wavelength can be acquired and we can extract the power transmission a_{eff} and effective delay time τ_{eff} at certain wavelengths, as shown in equation:

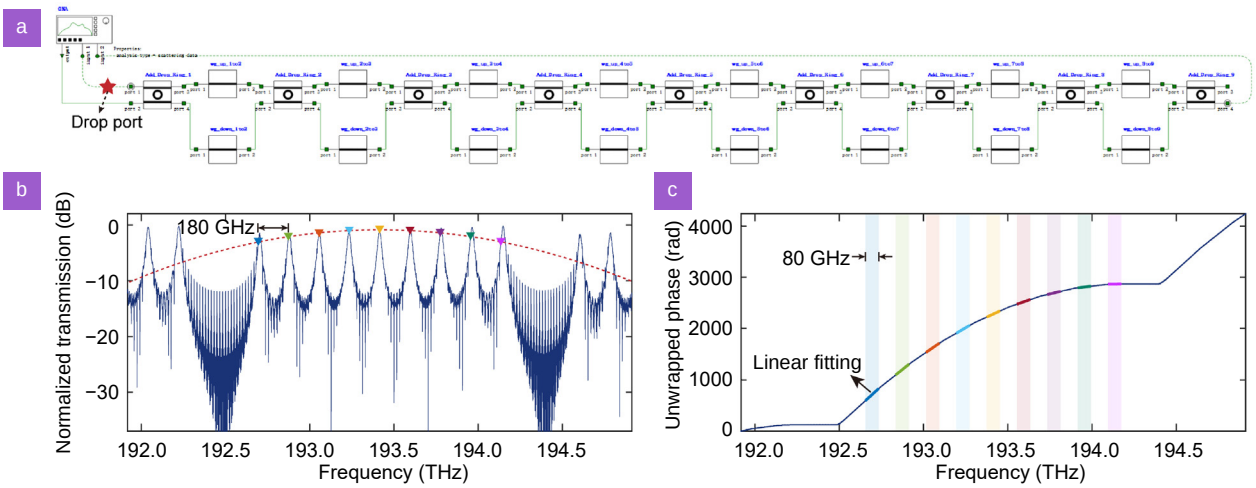

Fig. S5 | Simulation of the CMRR-DL system for MPF. (**a**) The model built in software. (**b**) Optical transmission power. (**c**) Optical transmission phase.

$$\tau_{\mathrm{eff},n} = \left.\frac{\mathrm{d}\varphi}{\mathrm{d}\Omega}\right|_{\Omega=\Omega_n}, \tag{S15}$$

where φ is the unwrapped optical phase and Ω is the optical angle frequency while Ω_n corresponds to the optical carrier. Then, the simulated RF transfer function can be acquired shown in Fig. S6. Comparing the RF responses under these 3 different conditions, we observed minimal differences, indicating that cross-talks can be neglected when the channel spacing and extinction ratio are sufficiently high.

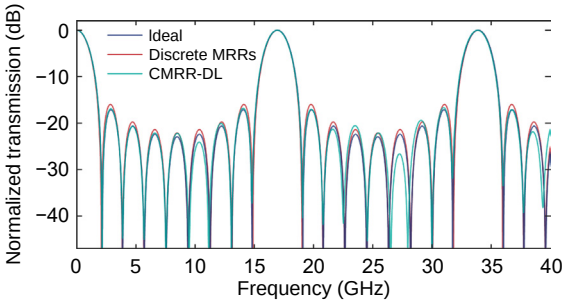

Fig. S6 | RF responses of the MPF in different models.

Section 4: The scalability of this architecture at different operating rates

The on-chip delay time is unchangeable once fabricated in our system and it affects the working rate. However, a deviation from a specific single rate does not render our system invalid. There is a tolerant range for the operating rate and various methods can be employed to compensate the deviation in the on-chip delay time.

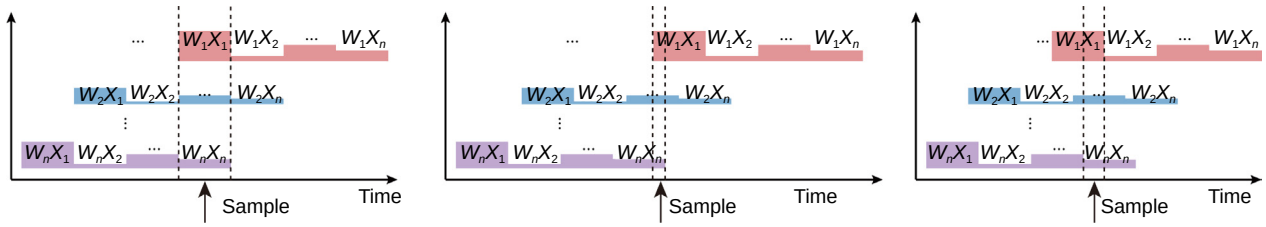

Fig. S7 | Situations that the delay time is equal to or larger/smaller than 1/*B*.

In computing and equalization applications, where the effective data come from sampling at specific time points, the system can function effectively as long as there is overlap for the relevant signals, as shown in Fig. S7. Assuming the number of taps is N and the on-chip delay time is τ, the operation rate B needs to satisfy the inequality as

$$(N-1)\cdot\frac{1}{B}<(N-1)\,\tau<N\cdot\frac{1}{B}\,. \tag{S16}$$

What's more, the fabrication process variations on delay lines also affect our system. Assuming the variation on the ith delay line is Δt_i, the condition that inter symbol crosstalk does not occur is

$$\begin{cases}\dfrac{(N-1)}{B}+\displaystyle\sum_{i=0}^{N-1}\Delta t_i<\dfrac{(N-1)}{B}+\dfrac{1}{2B}\\ \dfrac{N}{B}+\displaystyle\sum_{i=0}^{N-1}\Delta t_i>\dfrac{(N-1)}{B}+\dfrac{1}{2B}\end{cases}\rightarrow\left|\sum_{i=0}^{N-1}\Delta t_i\right|<\frac{1}{2B}\,. \tag{S17}$$

Theoretically speaking, if the total time delay variations is smaller than $1/2B$ the variations in different delay lines has little impact on the classification accuracy[S3].

In microwave photonics applications, the delay time determines the FSR of MPF. To achieve the delay time adjustment of the whole system, we can employ off-chip fiber with various dispersion property and length to compensate for the on-chip delay time.

It is notable that many works about the on-chip tunable delay lines have been reported based on the MZI optical switcher[S4] and cascaded MRRs[S5]. Introducing the tunable delay time architecture will enhance the scalability of our system in terms of operation rate and fabrication tolerance.

References

S1. Bogaerts W, De Heyn P, Van Vaerenbergh T et al. Silicon microring resonators. *Laser Photonics Rev* **6**, 47–73 (2012).
S2. Shu HW, Chang L, Tao YS et al. Microcomb-driven silicon photonic systems. *Nature* **605**, 457–463 (2022).
S3. Bai BW, Yang QP, Shu HW et al. Microcomb-based integrated photonic processing unit. *Nat Commun* **14**, 66 (2023).
S4. Xie YW, Hong SH, Yan H et al. Low-loss chip-scale programmable silicon photonic processor. *Opto-Electron Adv* **6**, 220030 (2023).
S5. Shan WS, Lu LJ, Wang XY et al. Broadband continuously tunable microwave photonic delay line based on cascaded silicon microrings. *Opt Express* **29**, 3375–3385 (2021).